

Supporting information

A polypyrrole-mediated photothermal biosensor with temperature and pressure dual readout for detection of protein biomarkers

Eunyeong Song ^a, Yingzhou Tao ^c, Haicong Shen ^a, Chaoyong Yang ^a, Tian Tian ^{b*}, Liu Yang ^{a*}, and Zhi Zhu ^{a*}

a. MOE Key Laboratory of Spectrochemical Analysis & Instrumentation, The Key Laboratory of Chemical Biology of Fujian Province, State Key Laboratory of Physical Chemistry of Solid Surfaces, Collaborative Innovation Center of Chemistry for Energy Materials, Department of Chemical Engineering, Department of Chemical Biology, College of Chemistry and Chemical Engineering, Xiamen University, Xiamen 361005, China

b. Chemistry and Biomedicine Innovation Center (ChemBIC), School of Chemistry and Chemical Engineering, Nanjing University, Nanjing, 210023, China

c. Integrated Chinese & Western Medicine Oncology Research Center, Jiangxi University of Chinese Medicine, Nanchang, Jiangxi, 330004, China

* To whom correspondence should be addressed. Tel: (+86) 592-218-7601, E-mail: zhuzhi@xmu.edu.cn, yangliu@xmu.edu.cn, tiantian@nju.edu.cn

Implementation of temperature and pressure-based photothermal performance

As shown in **Fig. S1**, the ELISA well container, PMMA lid, ELISA well and rubber were prepared to detect the temperature and pressure changes by a thermometer and a gas pressure meter under the 808nm laser irradiation. The ELISA well container for the photothermal performance was produced by a three-dimensional (3D) printer using ABS (Acrylonitrile-butadiene-styrene) material. The size of the container was 5x1.5x2 cm. The ELISA well was placed in a ELISA well container and covered with a thin rubber layer and a PMMA lid to seal the tube. This container was designed to increase the sensitivity of photothermal effects by sealing the well and stabilizing the device for laser irradiation. The ELISA well was horizontally irradiated by the 808nm laser. During irradiation, a digital thermometer sensor and a pressure meter needle were inserted through a hole in the PMMA lid to record the temperature changes ($^{\circ}\text{C}$) and pressure changes (kPa).

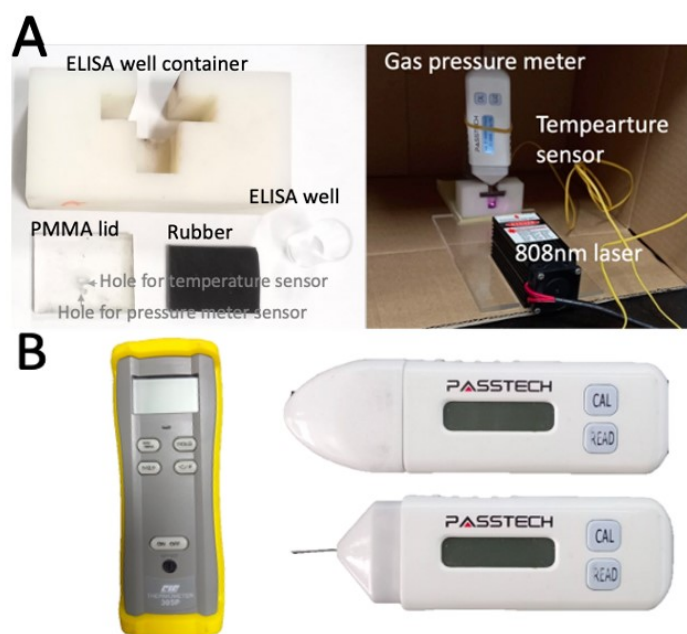


Fig. S1 Image of photothermal sensor. (A) components of the photothermal sensor and implementation of temperature and pressure-based photothermal performance under 808nm laser irradiation; (B) the digital thermometer for temperature signal readout and pressure meter for pressure signal readout

Investigation on the photothermal stability

In order to investigate the repeatability and photothermal stability of this system, 5 laser on/laser off cycles (on for 9 min; off for 5 min) . Under the 808 nm laser irradiation for 9 min and cooling for 5 min, the temperature was measured. As shown in **Fig. S2A**, the polypyrrole-based photothermal system demonstrated good photothermal stability and repeatability, which is one of essential properties for photothermal biosensors with practical applications.

According to literature reports, other traditional photothermal agents are known to have photo bleaching effects. For example, systems containing indocyanine green¹ and Au nanorods² showed decreased temperature elevation with increased laser irradiation cycles, because of fluorophore photo bleaching and melting of the Au nanorod under the NIR laser irradiation, respectively. Moreover, the UV-Vis spectrum of polypyrrole was monitored before and after laser irradiation for 5 min (**Fig. S2B**) and showed only minor changes in the absorbance peak of polypyrrole because of the high structural stability of polypyrrole³.

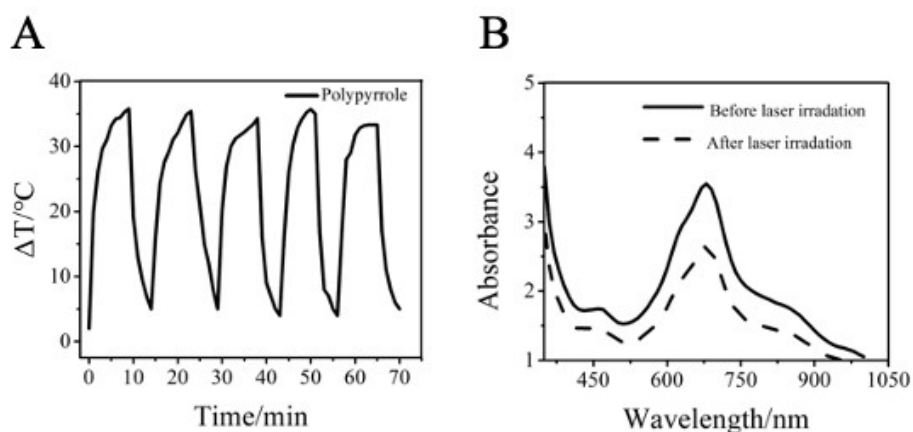


Fig. S2 (A) Photothermal variation of Polypyrrole after 5 laser on/off cycles. (B) UV vis-spectra of polypyrrole before and after laser irradiation with a power density for 0.2W/cm² for 5 min

The effect of Fe³⁺ in pyrrole polymerization

To evaluate the effect of Fe³⁺ in pyrrole polymerization for photothermal performance, different concentrations of Fe³⁺ were tested and the temperature and pressure signals were monitored after laser irradiation for 10 min with a power density of 0.2W/cm². The color of solutions became darker with increasing concentrations of Fe³⁺ (**Fig. S3A**), indicating the generation of polypyrrole. As shown in **Fig. S3A** and **Fig. S3C**, the temperature and pressure signals were observed in the range of 0-7 mM Fe³⁺. Temperature signals steadily increased with the increase of Fe³⁺ concentration, and pressure signals increased in parallel. Because the temperature and pressure signals reached their maxima within 9 min, 9 min laser irradiation was selected in subsequent experiments. As shown in **Fig. S3B** and **Fig. S3D**, calibration curves in temperature and pressure variations were linear in a range from 0 to 4 mM Fe³⁺ with R²=0.98816 and R²=0.99036, respectively. As 4 mM Fe³⁺ showed the maximum temperature and pressure signal changes in the linear dynamic range (LDR), for further experiments, 4 mM

Fe^{3+} was selected for sufficient pyrrole polymerization over the widest ranges of temperature and pressure signal readouts.

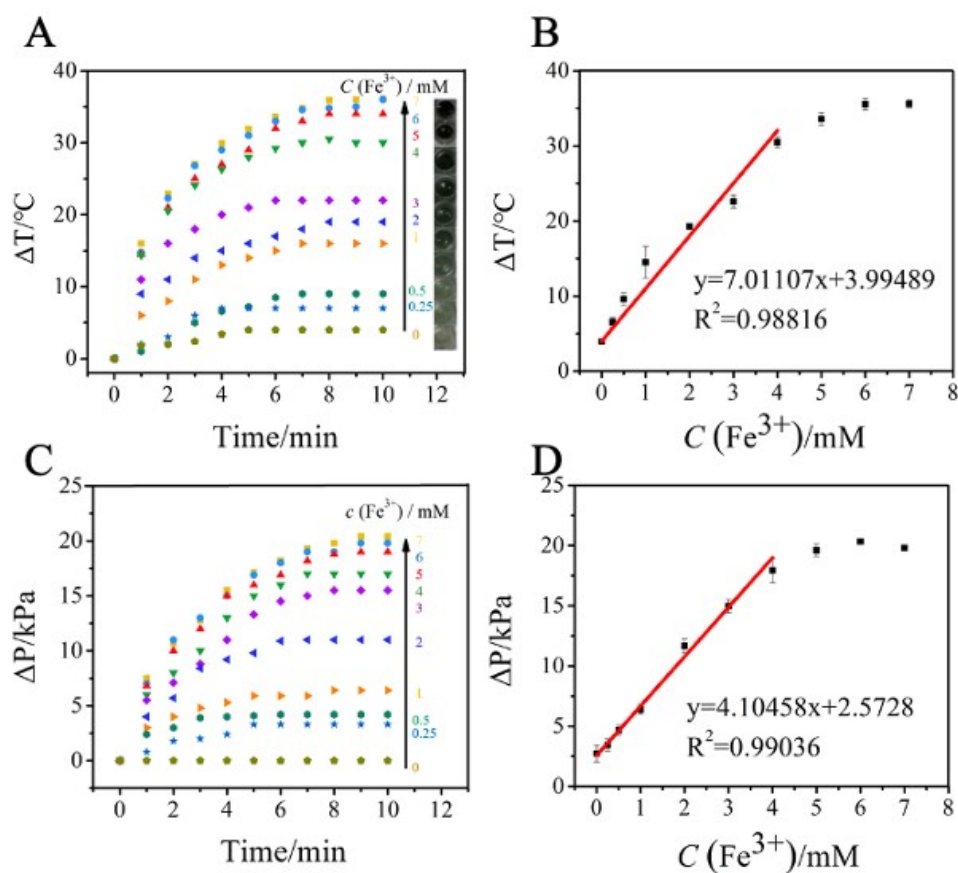


Fig. S3 Fe^{3+} effects on polypyrrole mediated photothermal performance. (A) temperature variation (B) calibration curve of temperature (C) pressure variation (D) calibration curve of pressure changes

Metal selectivity

To evaluate metal selectivity for polypyrrole, different ions (Al^{3+} , Na^+ , K^+ , Zn^{2+} , Mg^{2+} and Fe^{3+}) were tested in the same way with as the Fe^{3+} effect test, and temperature and pressure signals were recorded with a thermometer and pressure meter. Each metal ion was added to HCl and pyrrole suspensions at a final concentration of 20 mM and suspensions were irradiated with the 808nm laser for 10 min. **Fig. S4** show temperature and pressure variations after 10 min of laser irradiation. Inserted photography shows no obvious color changes metal ions other than Fe^{3+} . No obvious temperature and pressure variations were observed for ions other than Fe^{3+} , indicating that polypyrrole is produced only by Fe^{3+} , and not other ions. Therefore, polypyrrole polymerization was controlled with Fe^{3+} for temperature and pressure -based photothermal performance.

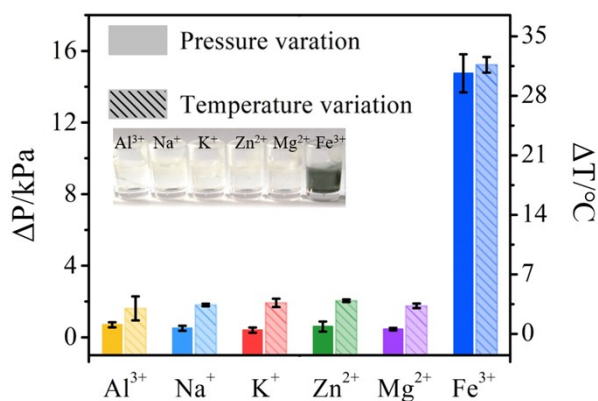


Fig. S4 Metal selectivity test of polypyrrole-mediated photothermal performance with temperature and pressure variation. Inset: photo image of samples

Irradiation setup

The irradiation setup for photothermal immunoassay was adjusted to achieve efficient photothermal effects using NIR laser irradiation (**Fig. S5**). Organic nanoparticles enable photothermal performances with a low laser power density, which is even lower than that of other metallic nanoparticles- (e.g., gold) mediated photothermal performance with similar light-to-heat conversion efficiency⁴. Different power densities (0.1W/cm², 0.2W/cm² and 0.45W/cm²) were monitored to induce suitable temperature and pressure changes in the photothermal biosensor system. The power density of 0.45W/cm² did not induce strong photothermal effects on temperature and pressure variations. On the contrary, 0.2W/cm² was observed with enhanced photothermal performance in temperature and pressure variations, as observed by other researchers^{5, 6}. As 0.2W/cm² showed strong photothermal performance in temperature and pressure elevations, the density of 0.2W/cm² was applied for further experiments.

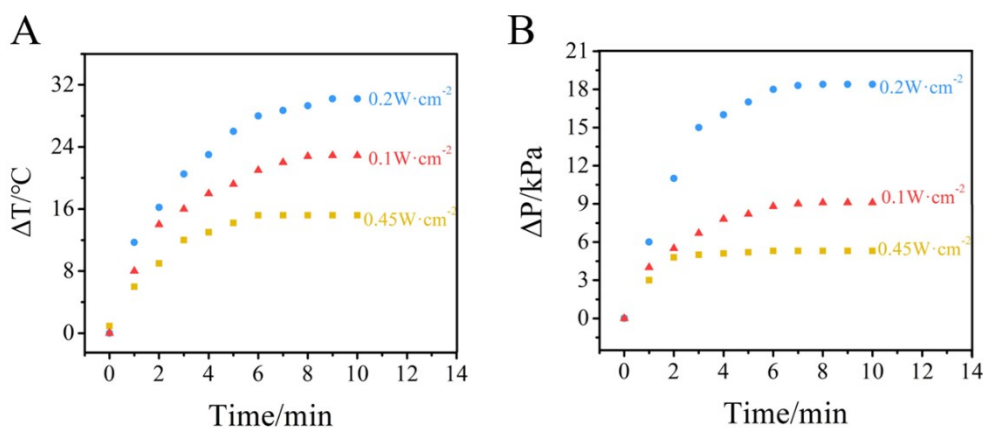


Fig. S5 Irradiation setup for (A) temperature and (B) pressure-based photothermal biosensor with the 808 nm laser.

Optimization of HCl concentration

To optimize HCl concentrations, different concentrations of HCl from 0 M to 2 M were used (Fig. S6). HCl was applied to disintegrate Fe₂O₃ in the CRP immunoassay, resulting in temperature and pressure increases when HCl concentrations increased. Temperature and pressure signals were monitored for 10 min under 808 nm laser irradiation. The temperature reached over 30 °C using 1M HCl, and the pressure increased to 15 kPa at 1M HCl. For further experiments, 1M HCl was selected to avoid safety risks with high concentrations of HCl.

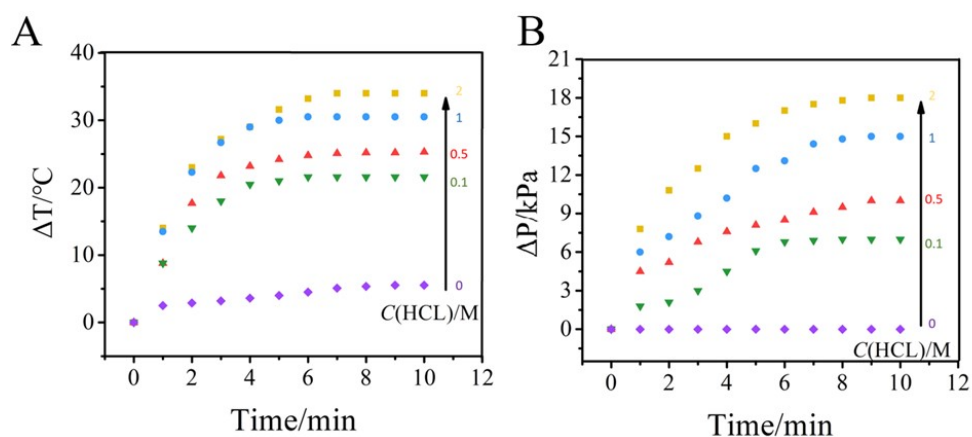


Fig. S6 Optimization of HCl concentration for polypyrrole mediated photothermal immunoassay

ELISA for CRP detection

ELISA was conducted to demonstrate applications of polypyrrole-mediated photothermal immunoassay. CRP concentrations in the range of 0.75mg/L to 12mg/L were tested (Fig. S7). First, 100 uL HRP-conjugate reagent was added to pre-coated micro-ELISA-wells and incubated for 60 min at 37 °C. Afterwards, each well was washed 5 times using 200 uL washing buffer. Then, 50 uL Chromogen solution A and 50 uL Chromogen solution B were added and incubated for 15 min at 37 °C. After adding 50 uL stop solution to each well, absorbances were recorded at 450 nm by spectrophotometry.

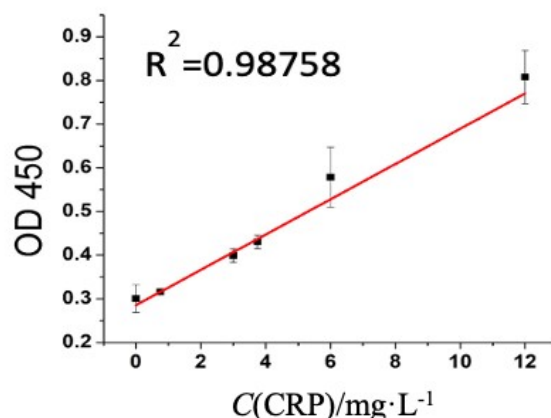


Fig. S7 Calibration curve of ELISA for CRP detection

Conjugation of Detection antibody-magnetic beads

Antibody-conjugated magnetic beads containing iron(III) were simply modified through biotin and streptavidin conjugation. Magnetic beads (200 μ L) were washed with PBS during magnetic separation. After resuspending the beads in PBS, 5 μ L biotinylated detection antibody (2 μ g/mL) was added and incubated for 30 min at room temperature with gentle rotation. Using a magnet, antibody-conjugated magnetic beads were separated and resuspended in PBS containing 0.1% BSA. To confirm the conjugation of detection antibody-magnetic beads, anti-FITC (fluorescein isothiocyanate) monoclonal antibody was bound to detection antibody and the conjugation was monitored by FACS (**Fig.S8**). Three solutions were prepared – magnetic beads, magnetic beads with added anti-FITC antibody, and magnetic beads with detection antibody conjugated anti-FITC antibody. As shown in **Fig. S8**, magnetic beads with detection antibody conjugated anti-FITC antibody displayed significant fluorescent signals, while unconjugated magnetic beads and magnetic beads with anti-FITC antibody did not, confirming the successful modification of detection antibodies on magnetic beads.

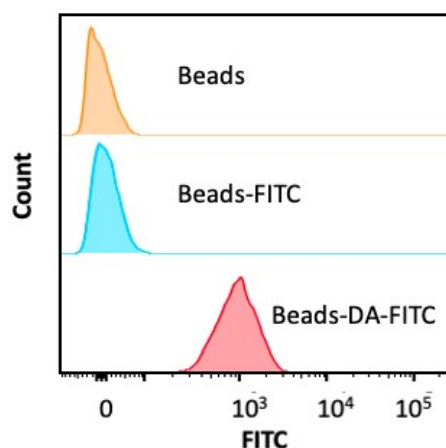


Fig. S8 Confirmation of magnetic bead conjugation with detection antibody

Emerging photothermal immunoassay

In recent years, photothermal bioassay has received increasing interest because of simple, easy, and rapid signal read-out. Various photothermal probes (e.g. Prussian blue nanoparticles, gold nanoparticles, oxidized TMB, etc.) have exhibited efficient absorption and conversion of light into heat energy in photothermal immunoassays, (Table S1). The advancement of photothermal probes in photothermal immunoassay will move forward as the number of photothermal-based immunoassay point of care tests becomes available. As temperature changes are consistent with analyte concentration, a thermometer or thermocouple has been applied for temperature signal read-out in photothermal immunoassay. But more accurate photothermal immunosensing devices are needed because of the limitation of temperature response, with only one decimal place on commercial thermometers and narrow ranges from 0 to approximately 30°C⁷. Herein, we developed dual signal readout system from temperature and pressure-based photothermal immunoassay with the polypyrrole photothermal probe in order to enhance the accuracy of the determination.

Table S1 Emerging photothermal immunoassay

Photothermal agents	Laser irradiation	Signal read-out	Reference
Prussian blue nanoparticle	808nm	Thermometer	8
Prussian blue nanoparticle encapsulated nanoliposomes	808nm	Thermometer	9
Gold nanoparticle	532nm	Photothermal biosensor	10
Gold nanoparticle	808nm	Thermal infrared imager	11
Glutathione-covered Au nanoparticles	808nm	Thermocouple	12
Cu ₃ (PO ₄) ₂ @Polydopamine	808nm	Thermometer	13
Ox-TMB	808nm	Thermometer	14
Au@Ag	450nm	Thermometer	15
Plasmonic Cu _{2-x} Se nanocrystals	808nm	Thermometer	5

References

1. Hu, S.; Tong, L.; Wang, J.; Yi, X.; Liu, J., NIR Light-Responsive Hollow Porous Gold Nanospheres for Controllable Pressure-Based Sensing and Photothermal Therapy of Cancer Cells. *Analytical Chemistry* **2019**, *91* (24), 15418-15424.
2. Fu, G.; Liu, W.; Feng, S.; Yue, X., Prussian blue nanoparticles operate as a new generation of photothermal ablation agents for cancer therapy. *Chemical Communications* **2012**, *48* (94), 11567-11569.
3. Wei, Y.; Wang, D.; Zhang, Y.; Sui, J.; Xu, Z., Multicolor and photothermal dual-readout biosensor for visual detection of prostate specific antigen. *Biosensors and Bioelectronics* **2019**, *140*, 111345.
4. Cheng, L.; Yang, K.; Chen, Q.; Liu, Z., Organic Stealth Nanoparticles for Highly Effective in Vivo Near-Infrared Photothermal Therapy of Cancer. *ACS Nano* **2012**, *6* (6), 5605-5613.
5. Li, X.; Yang, L.; Men, C.; Xie, Y. F.; Liu, J. J.; Zou, H. Y.; Li, Y. F.; Zhan, L.; Huang, C. Z., Photothermal Soft Nanoballs Developed by Loading Plasmonic Cu₂-xSe Nanocrystals into Liposomes for Photothermal Immunoassay of Aflatoxin B1. *Analytical Chemistry* **2019**, *91* (7), 4444-4450.
6. Zhang, D.; Du, S.; Su, S.; Wang, Y.; Zhang, H., Rapid detection method and portable device based on the photothermal effect of gold nanoparticles. *Biosensors and Bioelectronics* **2019**, *123*, 19-24.
7. Huang, L.; Chen, J.; Yu, Z.; Tang, D., Self-Powered Temperature Sensor with Seebeck Effect Transduction for Photothermal-Thermoelectric Coupled Immunoassay. *Analytical Chemistry* **2020**, *92* (3), 2809-2814.
8. Fu, G.; Sanjay, S. T.; Dou, M.; Li, X., Nanoparticle-mediated photothermal effect enables a new method for quantitative biochemical analysis using a thermometer. *Nanoscale* **2016**, *8* (10), 5422-5427.
9. Zhi, L.-J.; Sun, A.-L.; Tang, D., In situ amplified photothermal immunoassay for neuron-specific enolase with enhanced sensitivity using Prussian blue nanoparticle-loaded liposomes. *Analyst* **2020**, *145* (12), 4164-4172.
10. Lee, S. H.; Choi, S.; Kwon, K.; Bae, N.-H.; Kwak, B. S.; Cho, W. C.; Lee, S. J.; Jung, H.-I., A photothermal biosensor for detection of C-reactive protein in human saliva. *Sensors and Actuators B: Chemical* **2017**, *246*, 471-476.
11. Su, L.; Chen, Y.; Wang, L.; Zhang, H.; Sun, J.; Wang, J.; Zhang, D., Dual-signal based immunoassay for colorimetric and photothermal detection of furazolidone. *Sensors and Actuators B: Chemical* **2021**, *331*, 129431.
12. Liu, Y.; Pan, M.; Wang, W.; Jiang, Q.; Wang, F.; Pang, D.-W.; Liu, X., Plasmonic and Photothermal Immunoassay via Enzyme-Triggered Crystal Growth on Gold Nanostars. *Analytical Chemistry* **2019**, *91* (3), 2086-2092.
13. Tan, X.; Wang, X.; Zhang, L.; Liu, L.; Zheng, G.; Li, H.; Zhou, F., Stable and Photothermally Efficient Antibody-Covered Cu₃(PO₄)₂@Polydopamine Nanocomposites for Sensitive and Cost-Effective Immunoassays. *Analytical Chemistry* **2019**, *91* (13), 8274-8279.
14. Zhang, B.; Jia, Y.; Wang, J.; Chang, H.; Zhao, Z.; Cheng, Y., Colorimetric and photothermal dual-mode immunoassay for tumour marker detection based on a Ag₂CO₃@Ag nanocomposite. *Process Biochemistry* **2019**, *87*, 66-72.
15. Tao, Y.; Lin, Y.; Luo, F.; Fu, C.; Lin, C.; He, Y.; Cai, Z.; Qiu, B.; Lin, Z., Convenient detection of H₂S based on the photothermal effect of Au@Ag nanocubes using a handheld thermometer as readout. *Analytica Chimica Acta* **2021**, *1149*, 338211.